Proc. Natl. Acad. Sci. USA
Vol. 77, No. 4, pp. 2028–2032, April 1980
Biophysics

Rate theory calculation of gramicidin single-channel currents using NMR-derived rate constants

(²³Na NMR/transmembrane currents/sodium binding/ion transport)

DAN W. URRY*, C. MAHALINGAM VENKATACHALAM*, ALBERTO SPISNI*, PETER LÄUGER†, AND MD. ABU KHALED*

*Laboratory of Molecular Biophysics, University of Alabama Medical Center, Birmingham, Alabama 35294; and †Fachbereich Biologie, Universität Konstanz, Postfach 7733, Konstanz, West Germany

Communicated by Henry Eyring, January 11, 1980

ABSTRACT **By means of ²³Na NMR, two ion binding sites were observed in phospholipid-packaged gramicidin channels and the four associated rate constants were approximated. Limits also were placed on a fifth rate constant for an intrachannel ion translocation. By using Eyring rate theory to introduce voltage dependence, these rate constants were used in steady-state-current equations for calculation of gramicidin single-channel currents for two- and three-site models. Calculated single-channel currents are compared with previously published experimental single-channel currents obtained by electrical measurements on Na^+ transport across gramicidin-doped planar lipid bilayers. The calculated results for the two- and three-site models compare favorably with the experimental results. Accordingly, it is demonstrated that NMR-derived rate constants can be coupled with Eyring rate theory to calculate currents through a transmembrane channel and to do so within levels of variation that compare with the differences obtained on planar lipid bilayers formed with different lipids.**

Gramicidin A (GA), a hydrophobic linear pentadecapeptide [HCO-L-Val-Gly-L-Ala-D-Leu-L-Ala-D-Val-L-Val-D-Val-L-Trp-D-Leu-L-Trp-D-Leu-L-Trp-D-Leu-L-Trp-NHCH$_2$CH$_2$OH (1)], effects conductance of cations across planar lipid bilayer membranes (2) by means of discrete increments (3–5). The conductance steps are due to the formation of a continuous transmembrane channel (5, 6), with a single transmembrane channel being capable of conducting 10^7 ions/sec at 1 M salt, 100 mV transmembrane potential, and 25°C (7, 8). This is a single-channel conductance of the order of 10 pS.

As proposed in 1971 (9, 10) and now widely accepted (11, 12), the transmembrane channel is formed from the formyl-to-formyl hydrogen-bonded dimerization of two helical monomers containing 6.3 residues per turn and a 4 Å diameter channel (Fig. 1). The length of the channel is about 26 Å (see figure 6 of ref. 13 and $\beta^6_{3,3}$-helix parameters of ref. 14) and there is a 2-fold symmetry axis perpendicular to the channel axis. The diameter of the channel and the properties of the channel walls cause water and cations to pass through the channel in single file (15).

Recent x-ray diffraction studies (16) on a cation-containing gramicidin structure, although at low resolution, are in excellent agreement with the previously described structure (10, 14), within tenths of an angstrom of channel length and helix radius. The cation-binding sites (two sites per channel) are separated by 21 Å and 5 Å. Under the conditions of crystallization, this identifies what are referred to in the present paper as the tight-binding sites. With a 26-Å-length to the channel, this places the binding sites 2.5 Å in from one end of a monomer but from which end, the ethanolamine end or the formyl end, is not determined. In the former case the tight-binding sites would be 2.5 Å in from the mouths (ethanolamine ends) of the channel separated by 21 Å; in the latter case, the tight-binding sites would be at the center of the channel (formyl ends) separated by 5 Å, in which case the situation would be a doubly degenerate site but with only single occupancy of this site being possible. Because one turn of helix is 5 Å, the 2.5-Å distance in from either end of the monomer places the cation exactly at the center of a terminal turn of helix.

It has recently been demonstrated that functional gramicidin channels can be packaged in lipid micelles (17, 18). This allows for spectroscopic characterization during ion titrations without the development of complicating electrochemical gradients that would make difficult the analysis of cation interactions with channels incorporated into lipid vesicles. Interestingly, the energy of activation for sodium exchange with the micellar channel, at approximately equimolar sodium and channel concentrations, is essentially the same as the overall energy of activation for transport through the channel (19). Accordingly, any other translocation rate for movements within the channel are taken to be faster than the off-rate from the tight-binding site.

The first rate analysis of ion transport through the gramicidin channel was carried out by Läuger (20). Subsequently, calculations of single-channel currents have been carried out by Hladky *et al.* (21) and by Sandblom *et al.* (22) using two- and four-site models, respectively, and using five or more fitted parameters.

In the present work it is shown that four rate constants derived from ²³Na NMR studies plus a fifth rate constant, limited as noted immediately above, can be used, when Eyring rate theory is used to introduce voltage dependence, to calculate gramicidin single-channel currents for two- and three-site models that satisfactorily compare with the experimental results.

NMR-derived rate constants

Following a procedure reported elsewhere (17, 18), GA was incorporated into lysolecithin micelles. ²³Na chemical shift, δ(ppm) (or ν in Hz), line widths ($\nu_{1/2}$), and longitudinal (T_1) and transverse (T_2) relaxation times were obtained as a function of ²³Na concentrations by using a JEOL FX-100 equipped with a multinuclear probe operating at 26.3 MHz.

Excess Longitudinal Relaxation Rate Plot as Evidence for Multiple Binding. The longitudinal relaxation time (T_1) or its inverse, the longitudinal relaxation rate (R_1), for Na exchanging between a free solution state f and a bound state b is $R_1 = T_1^{-1} = P_f R_{1f} + P_b R_{1b}$. In this case, as shown by James and Noggle (23), a plot of the reciprocal of the excess relaxation rate, $(R_1 - R_{1f})^{-1}$, against Na concentration will be a straight line extrapolating to give an x-axis intercept of $-K_b^{-1}$ when Na concentration is sufficiently greater than the site concentration (24). Fig. 2 shows such a plot for GA with Na concentration ranging

The publication costs of this article were defrayed in part by page charge payment. This article must therefore be hereby marked "*advertisement*" in accordance with 18 U. S. C. §1734 solely to indicate this fact.

Abbreviation: GA, gramicidin A.

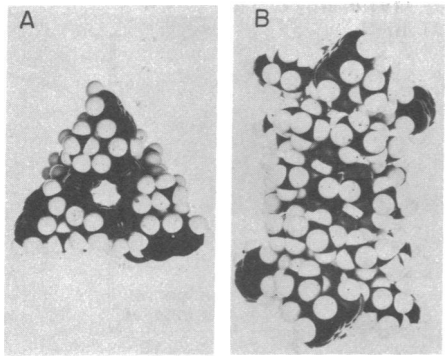

FIG. 1. Gramicidin transmembrane structure. (*A*) Channel view. (*B*) Side view. [From Urry *et al.* (13), by permission.]

from 5 to 350 mM. The most striking feature of this plot is that the data points are approximated by two different straight lines, indicating the presence of two distinguishable binding sites in the channel. The tighter-binding site is seen at the lower concentrations and the weaker-binding site, at higher concentrations. The x-axis intercepts of the two lines yield apparent binding constants of $K_b^t \approx 20\ M^{-1}$ for the tight-binding site and $K_b^w \approx 5\ M^{-1}$ for the weak-binding site. The actual binding constants may be different because the intercepts from the plot of two overlapping binding processes generally tend to underestimate the tight-binding site and overestimate the weak-binding site. If P_t and P_w are the fractions of ions bound to tight-binding and weak-binding sites, respectively, then

$$(R_1 - R_{1f}) = P_t(R_{1t} - R_{1f}) + P_w(R_{1w} - R_{1f}). \quad [1]$$

Actual binding constants and T_1s at the two types of sites may be obtained by least-square fitting of the data in Fig. 2 to Eq. 1. The relationship between fractions bound (P_t, P_w) and the binding constants (K_b^t, K_b^w) depends on the nature of the multiple occupancy model considered.

Chemical Shifts and Line Widths to Determine Off-Rate Constant from Tight-Binding Site, k_{off}^t. Fig. 3 shows the observed variation, with Na concentration of ^{23}Na chemical shift, ν (in Hz), and line width, $\nu_{1/2}$ (in Hz). The object here is to obtain K_b^t and the off-rate, k_{off}^t, of the tight-binding site by using the low-concentration data. If the fast-exchange condition prevails for the tight-binding site, then (25)

$$\nu = P_f\nu_f + P_t\nu_t \quad \text{and} \quad [2]$$

$$\nu_{1/2} = \nu_{1/2}^f + P_t(\nu_{1/2}^t - \nu_{1/2}^f) + 4\pi P_t(1 - P_t)^2 \frac{\nu_t^2}{k_{off}^t}. \quad [3]$$

By combining Eqs. 2 and 3, P_t is eliminated to obtain a relationship between ν and $\nu_{1/2}$. By using a one-site model for the tight-binding site at low Na concentration, K_b^t and ν_t are obtained by fitting the chemical shift data to Eq. 2. $\nu_{1/2}^t$ and k_{off}^t are obtained by using Eq. 3 and the line-width data.

The assumption of fast exchange has been checked by using more general expressions (see for instance, equations **9, 10,** and **11** of ref. 25) to obtain an essentially identical result. Calculated curves for chemical shift and line width as a function of Na concentration are included in Fig. 3, for the tight-binding site of the two-site model to show how well the experimental data can be fitted.

Fig. 3 *Inset* shows the data plotted as $\nu_{1/2}$ vs ν. Shown are calculated plots using general expressions valid for intermediate exchange (25) for various values of k_{off}^t. The data points coincide with the calculated plot for $k_{off}^t \approx 3 \times 10^5$/sec. Variability in gramicidin incorporation into the micelles and sensitivity limitations at low Na concentration limit the estimate of k_{off}^t to $10^{5.5 \pm 0.5}$/sec.

Determination of Off-Rate Constants, k_{off}^w, for the Weak-Binding Site by Using Relaxation Time Measurements at High Na Concentrations. Measurement of longitudinal and transverse relaxation times enables computation of the correlation time, τ_c, of the ion at the weak-binding site from which the off-rate, k_{off}^w, is obtained because $1/\tau_c \approx 1/\tau_b^w = k_{off}^w$ (26).

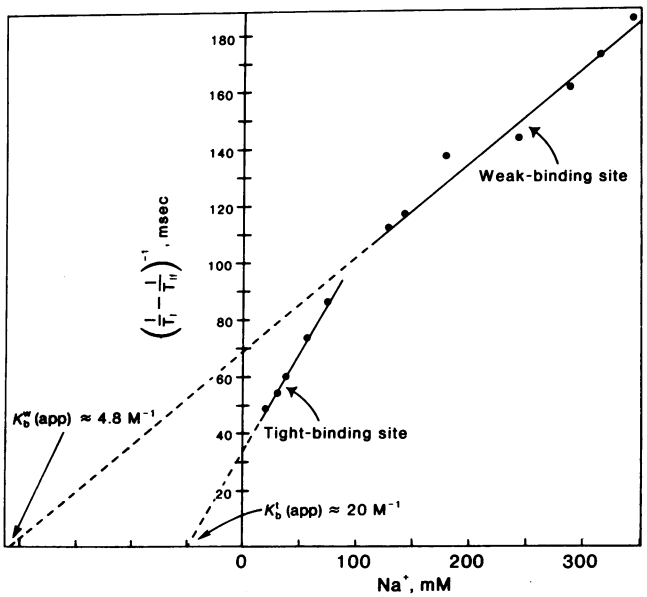

FIG. 2. Plot of reciprocal of excess relaxation rate against ^{23}Na concentration, with GA ≈3 mM T_{1f} ≈49 msec for the GA-free micellar system. The "break" in the plot around 100 mM, resulting in two different lines, argues for two binding sites on GA. The extrapolated x-axis intercepts give only "apparent" binding constants for the two sites.

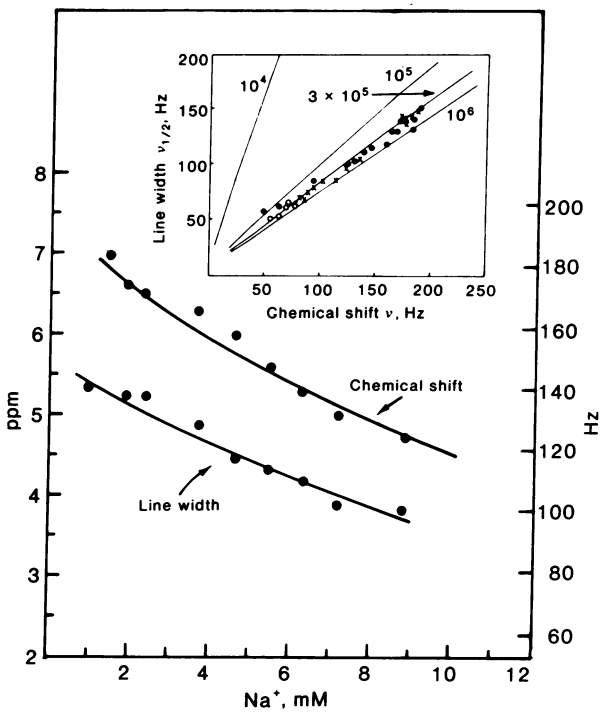

FIG. 3. Variation of chemical shift and line width with Na concentration, at GA ≈2 mM for one series of ion titrations. Theoretically calculated curves (by using ν_t ≈2000 Hz and $\nu_{1/2}^t$ ≈400 Hz) are shown for a two-site model. (*Inset*) $\nu_{1/2}$ vs. ν plot. The shape of this plot is independent of the binding constant and also of the effective concentration of the incorporated GA. Theoretically calculated plots for various values of k_{off}^t are shown. The experimental points here include several sets of titrations with different concentrations of GA.

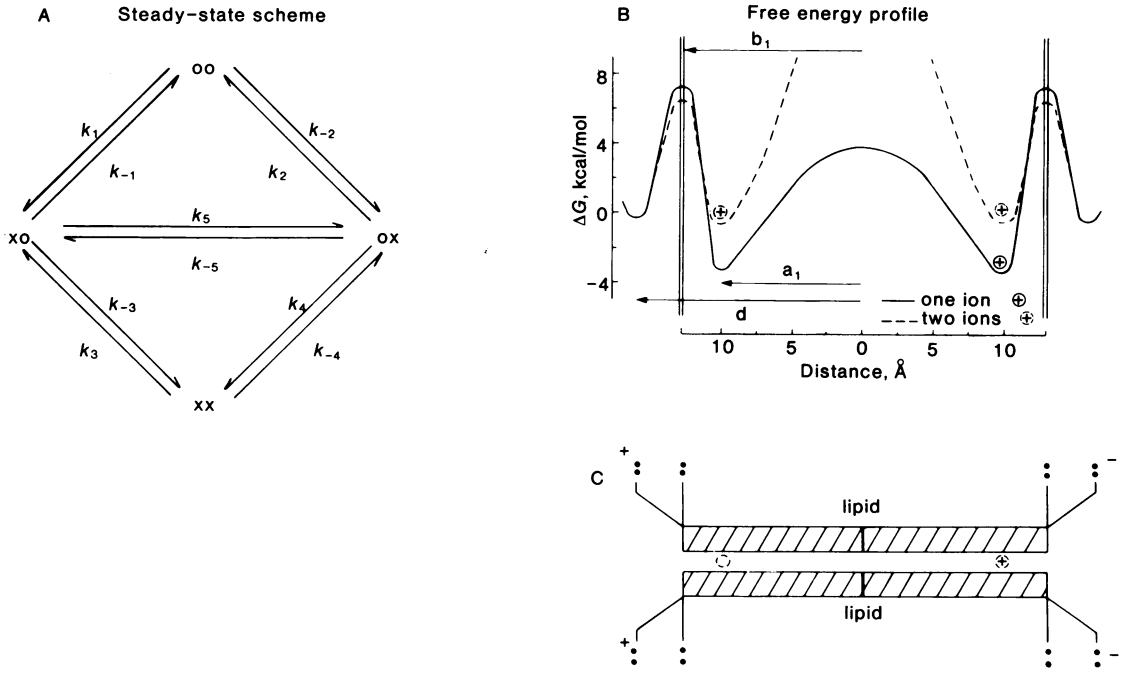

FIG. 4. Two-site model. The free energy profile was calculated from the experimental rate constants by using Eyring rate theory. The steady-state equations are as follows:

$$\dot{\chi}(\mathrm{oo}) = -(C'_\chi k_1 + C''_\chi k_{-2})\chi(\mathrm{oo}) + k_{-1}\chi(\mathrm{xo}) + k_2\chi(\mathrm{ox}) = 0.$$

$$\dot{\chi}(\mathrm{xo}) = C'_\chi k_1\chi(\mathrm{oo}) - (k_{-1} + k_5 + C''_\chi k_{-3})\chi(\mathrm{xo}) + k_{-5}\chi(\mathrm{ox}) + k_3\chi(\mathrm{xx}) = 0.$$

$$\dot{\chi}(\mathrm{ox}) = C''_\chi k_{-2}\chi(\mathrm{oo}) + k_5\chi(\mathrm{xo}) - (k_2 + k_{-5} + C'_\chi k_4)\chi(\mathrm{ox}) + k_{-4}\chi(\mathrm{xx}) = 0.$$

$$\dot{\chi}(\mathrm{xx}) = C''_\chi k_{-3}\chi(\mathrm{xo}) + C'_\chi k_4\chi(\mathrm{ox}) - (k_3 + k_{-4})\chi(\mathrm{xx}) = 0.$$

The current is given by:

$$I_\chi = (ze/2d)\{(d - a_1)(C'_\chi k_1 - C''_\chi k_{-2})\chi(\mathrm{oo}) + [2a_1k_5 - (d - a_1)(k_{-1} + C''_\chi k_{-3})]\chi(\mathrm{xo}) + [(d - a_1)(k_2 + C'_\chi k_4) - 2a_1k_{-5}]\chi(\mathrm{ox}) + (d - a_1)(k_3 - k_{-4})\chi(\mathrm{xx})\}.$$

At Na ≈ 350 mM and $T_1 \approx 26.2$ msec, the transverse relaxation is found to be nonexponential, as is expected of a quadrupole-relaxed nucleus (27). A T'_2 of ≈2 msec and a T''_2 of ≈16 msec were experimentally observed. The observation of both components results from the fact that the extreme narrowing condition is not satisfied at the binding site (26–29). Under these conditions, T'_2, T''_2, and τ_c are related by (29)

$$\frac{1/T'_2 - 1/T_{2f}}{1/T''_2 - 1/T_{2f}} = \frac{1 + 1/(1 + \omega^2\tau_c^2)}{1/(1 + 4\omega^2\tau_c^2) + 1/(1 + \omega^2\tau_c^2)}. \quad [4]$$

With $\omega = 16.5 \times 10^7$ rad/sec and $T_{2f} = 50$ msec, $\tau_c \approx 2.5 \times 10^{-8}$ sec, yielding $k^w_{off} \approx 4 \times 10^7$/sec.

Multiple occupancy models

The problem of multiple occupancy is approached without prejudgement as to the magnitude of the central barrier that may result from the low dielectric constant of the lipid and without prejudgement as to the repulsion between ions. The perspectives are taken from the structural data that there is single filing through a 26-Å channel and that there is a 2-fold symmetry axis perpendicular to the channel axis, from the x-ray data that the tight-binding site is 2.5 Å in from an end of the monomer, and from the NMR data that there are at least two sites of different affinity, that, where relevant, the tight-binding site is central to the weak site, and that no barrier is higher than the barrier faced by an ion leaving the channel from the tight-binding site.

Two-Site Model. Because of the 2-fold symmetry of the channel, both sites are necessarily identical. The tight-binding site would result from single occupancy at either site; the weak-binding site would result from repulsion on double occupancy. Fig. 4 contains the steady-state scheme and the steady-state equations in which, for example, $\chi(\mathrm{oo})$ is the probability of the unoccupied channel and C'_χ and C''_χ are the concentrations on the positive (left-hand) and negative (right-hand) sides of the membrane, respectively. Given the statistics of the two-site model, the binding constants from NMR data become $K^t_b \approx 100\ \mathrm{M}^{-1}$ and $K^w_b \approx 3\ \mathrm{M}^{-1}$. With the off-rate constants of $k^t_{off} = 3 \times 10^5$/sec and $k^w_{off} = 4 \times 10^7$/sec, this gives for the on-rate constants $k^t_{on} = 3 \times 10^7$/M·sec and $k^w_{on} = 1.2 \times 10^8$/M·sec. By means of identification at zero voltage, $k^t_{off} = k_{-1} = k_2$, $k^t_{on} = k_1 = k_{-2}$, $k^w_{off} = k_3 = k_{-4}$, $k^w_{on} = k_{-3} = k_4$, and $k_5 = k_{-5} > k^t_{off}$. The latter identification comes from the demonstration, noted in the *Introduction*, that at low concentration the temperature dependence of T_1 and of $\nu_{1/2}$ gives an $E_a \approx 7.1 \pm 0.3$ kcal/mol which is essentially the value, 7.3 kcal/mol, for transport through the channel for dioleoyl lecithin membranes (19). This is taken to mean that the central barrier can be no higher than the barrier for the off-rate from the tight-binding site. The free energy profile for permeation for this set of rate constants is given in Fig. 4*B*; a scale diagram of the channel is given below. The reaction coordinate for permeation, of course, coincides with the channel axis and the minima of the energy profile correspond with the positions of occupancy in the channel.

Three-Site Model. Given 2-fold symmetry, a three-site model would require the presence of binding in the region of the central head-to-head junction. On the basis of the x-ray data (16), the central site would be doubly degenerate as to a position 2.5 Å from the head end of each monomer, but we reject simultaneous occupancy. Also, for simplicity, an averaged position is taken at the junction. Because, at low ion concentration,

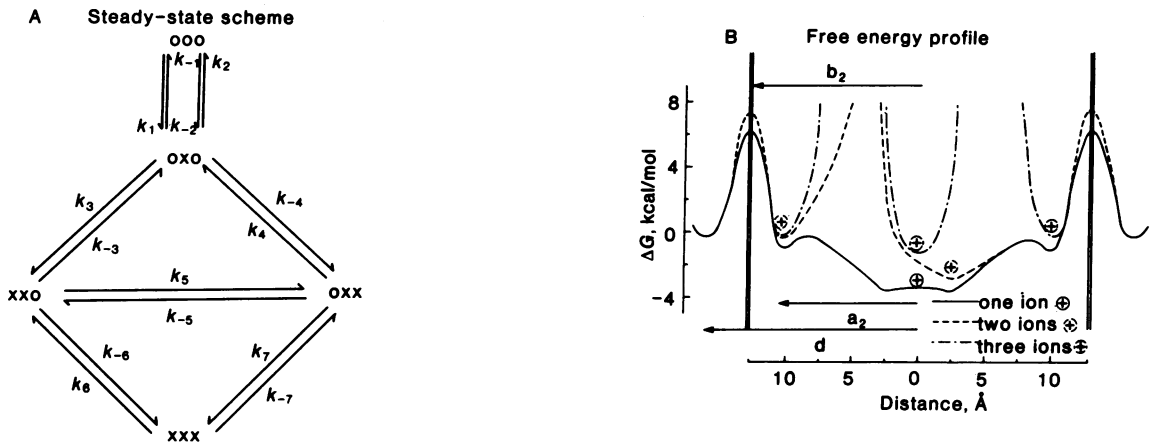

FIG. 5. Three-site model (virtual weak-binding sites). The steady-state equations are as follows:

$$\dot{\chi}(\text{ooo}) = -(C'_\chi k_1 + C''_\chi k_{-2})\chi(\text{ooo}) + (k_{-1} + k_2)\chi(\text{oxo}) = 0.$$

$$\dot{\chi}(\text{oxo}) = (C'_\chi k_1 + C''_\chi k_{-2})\chi(\text{ooo}) - (k_{-1} + k_2 + C'_\chi k_3 + C''_\chi k_{-4})\chi(\text{oxo}) + k_{-3}\chi(\text{xxo}) + k_4\chi(\text{oxx}) = 0.$$

$$\dot{\chi}(\text{xxo}) = C'_\chi k_3\chi(\text{oxo}) - (k_{-3} + C''_\chi k_{-6} + k_5)\chi(\text{xxo}) + k_{-5}\chi(\text{oxx}) + k_6\chi(\text{xxx}) = 0.$$

$$\dot{\chi}(\text{oxx}) = C''_\chi k_{-4}\chi(\text{oxo}) + k_5\chi(\text{xxo}) - (k_4 + k_{-5} + C'_\chi k_7)\chi(\text{oxx}) + k_{-7}\chi(\text{xxx}) = 0.$$

$$\dot{\chi}(\text{xxx}) = C''_\chi k_{-6}\chi(\text{xxo}) + C'_\chi k_7\chi(\text{oxx}) - (k_6 + k_{-7})\chi(\text{xxx}) = 0.$$

The current is given by:

$$I_\chi = (ze/2d)\{(dk_2 - dk_{-1})\chi(\text{oxo}) + [2a_2k_5 - (d - a_2)k_{-3}]\chi(\text{xxo}) + [(d - a_2)k_4 - 2a_2k_{-5}]\chi(\text{oxx}) + [(d - a_2)k_6 - (d - a_2)k_{-7}]\chi(\text{xxx}) + C'_\chi dk_1\chi(\text{ooo}) + C'_\chi(d - a_2)k_3\chi(\text{oxo}) + C'_\chi(d - a_2)k_7\chi(\text{oxx}) - C''_\chi dk_{-2}\chi(\text{ooo}) - C''_\chi(d - a_2)k_{-4}\chi(\text{oxo}) - C''_\chi(d - a_2)k_{-6}\chi(\text{xxo})\}.$$

a tight-binding site is observed and at high ion concentration a weak-binding site is observed with exchange properties faster than those for the tight-binding site, this requires that the tight-binding site be central, with the two weak-binding sites closer to the channel mouths. This is because of single filing. An ion in an inner weak-binding site could exchange no faster with solution than an ion in an outer tight-binding site because it would have to pass through the outer tight-binding site to reach the solution. On the other hand, once a more slowly exchanging tight-binding site were filled, another ion could still exchange rapidly with an outer site and equilibrate with the ions in solution. Also, because the tight-binding site is observed at low concentration with the slower exchange rate and the ion does not seem to be able to exchange rapidly with the outer weak-binding site, this implies that the weak-binding site is a virtual site, a metastable site, which does not become a stable binding position until the tight-binding site is occupied.

Given the structure of the channel, we would have to argue that, for a three-site model to be the correct model, the amino acid side chains make the difference. Perhaps the presence of alanines and a glycine at the formyl end allows for a more energetically favorable libration of peptide moieties for coordination of the ion than at the ethanolamine end where the amino acids are leucine and tryptophan with bulky side chains. Retaining, however, the perspective that the first turn of helix makes a favorable binding site, the weak-binding site is placed 2.5 Å in from the ethanolamine end. The steady-state scheme, equations, and free energy profile are in Fig. 5 which utilizes the above arguments and the following rate constants.

With the effective concentrations of weak- and tight-binding sites for a three-site model, the binding constants become $K_b^t \approx 300\ M^{-1}$ and $K_b^w \approx 1\ M^{-1}$. This gives the four rate constants $k_{off}^t \approx 3 \times 10^5$/sec, $k_{on}^t \approx 9 \times 10^7$/M·sec, $k_{off}^w \approx 4 \times 10^7$/sec, and $k_{on}^w \approx 4 \times 10^7$/M·sec. Because the NMR data do not distinguish between the filling of a first and a second weak-binding site, at zero potential, $k_3 = k_{-4} = k_{-6} = k_7 = k_{on}^w$, $k_{-3} = k_4 = k_6 = k_{-7} = k_{off}^w$, $k_1 = k_{-2} = k_{on}^t$, and $k_{-1} = k_2 = k_{off}^t$. Because of the virtual weak-binding site perspective, there can be the central shift xxo $\rightleftharpoons$ oxx, and because no rate can be slower than k_{off}^t (see *Introduction*), the rate constant for the central shift $k_{cs} = k_5 = k_{-5} > k_{off}^t$ at zero potential.

Rate theory calculation of single-channel currents

Development of Voltage-Dependent Rate Constants. The effect of a transmembrane potential on a channel spanning a planar lipid bilayer separating two aqueous chambers is to cause symmetrically related states—for example, the ox and xo states in the two-site model shown in Fig. 4—to become nonequiva-

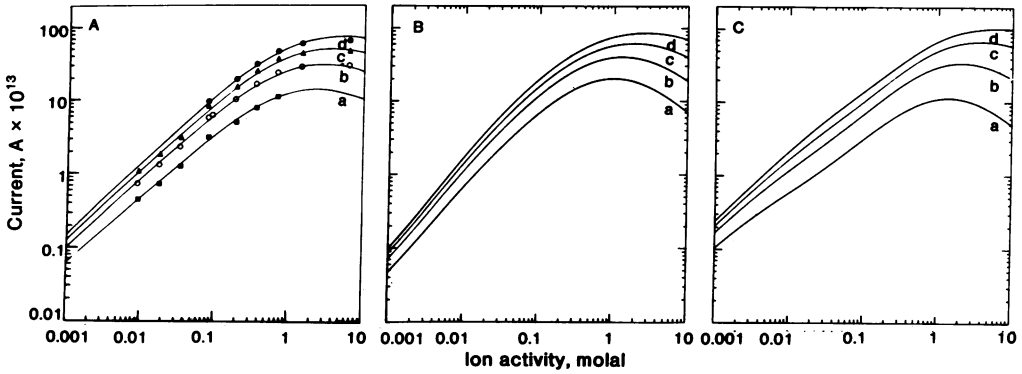

FIG. 6. Calculated single-channel currents for GA as a function of Na^+ concentration for various transmembrane potentials: curve a, 50 mV; curve b, 100 mV; curve c, 150 mV; curve d, 200 mV. (*A*) Hladky *et al.* (21), experimental data points and curves calculated from their five-parameter two-site model; (*B*) two-site model (general); (*C*) three-site model (virtual weak-binding site).

lent and rate constants—such as k_5 and k_{-5}—to become unequal. By utilizing the Eyring rate theory approach to the introduction of voltage dependence (30–33) with a transmembrane potential making the left-hand side positive and the right-hand side negative (see Fig. 4*C*), the rate constants for passage over the central barrier, which would be $k_{cb} = k_5 = k_{-5}$ in the absence of a potential, become $k_5 = k_{cb} \exp[a_1 zFU/2dRT]$ and $k_{-5} = k_{cb} \exp[-a_1 zFU/2dRT]$, in which $2d$ is the total length over which the potential is applied, a_1 is the distance from the binding site to the top of the central barrier, z is the charge on the ion, F is the Faraday, U is the transmembrane potential, R is the gas constant, and T is the absolute temperature. Defining the quantities $X \equiv \exp(zFU/2dRT)$, $\ell_1 = d - b_1$, and $\ell_2 = b_1 - a_1$ gives $k_1 = k^t_{on} X^{\ell_1}$, $k_{-1} = k^t_{off} X^{-\ell_2}$, $k_2 = k^t_{off} X^{\ell_2}$, $k_{-2} = k^t_{on} X^{-\ell_1}$, $k_3 = k^w_{off} X^{\ell_2}$, $k_{-3} = k^w_{on} X^{-\ell_1}$, $k_4 = k^w_{on} X^{\ell_1}$, $k_{-4} = k^w_{off} X^{-\ell_2}$, $k_5 = k_{cb} X^{a_1}$, and $k_{-5} = k_{cb} X^{-a_1}$.

Single-Channel Currents. Calculation of single-channel currents is approached with the steady-state and general current equations included in Figs. 4 and 5 for the two- and three-site models, respectively. At steady state, for example, considering the left-hand barrier of the two-site model, the single-channel current becomes

$$I = ze[Ck_1\chi(oo) - k_{-1}\chi(xo) + Ck_4\chi(ox) - k_{-4}\chi(xx)]. \quad [5]$$

The current equations are checked in three ways. The general equation is checked to agree exactly with each of the single-barrier equations; when the potential is set to zero, the current must be zero; and when the potential is reversed, the current is exactly reversed. Also, both a matrix method and explicit equations derived for the two- and three-site models were used and found to be in complete agreement. The explicit expressions were of the form developed by Sandblom *et al.* (22).

Comparison of Experimental and Calculated Single-Channel Currents. As formulated, five rate constants are required for calculation of the single-channel currents for the two models; of these, NMR yields four constants and a minimal value for the fifth. The fifth rate constant, k_{cb} for the two-site model and k_{cs} for the three-site model, is necessarily larger than the off-rate constant from the tight-binding site. Thus, the calculation is achieved with only one parameter but that parameter has been limited to a specific range of values, greater than 3×10^5/sec but less than 10^{10}/sec.

The experimental values of Hladky *et al.* (21) are replotted in Fig. 6*A* for comparison with the calculated curves in Fig. 6 *B* and *C* for the two- and three-site models, respectively. Given that the NMR-derived rate constants are not precise, these were subsequently allowed to vary in order to determine what similar values would provide a "best fit" for the 100-mV curve. The values are $k^w_{off} = 1.7 \times 10^7$, $k^w_{on} = 3.4 \times 10^7$, $k^t_{off} = 2.6 \times 10^5$, and $k^t_{on} = 5.2 \times 10^7$ for the three-site model and $k^w_{off} = 2 \times 10^7$, $k^w_{on} = 6 \times 10^7$, $k^t_{off} = 5.5 \times 10^5$, and $k^t_{on} = 5.5 \times 10^7$ for the two-site model. Surprisingly, the fitted values differed from the NMR-derived values by no more than a factor of about 2, and the fifth value remained within the allowed limits. Interestingly, a factor of 2 is the approximate difference observed between different lipids—that is, ≈25 pS is the conductance for glyceryl monooleate membranes at 1 M NaCl and 100 mV (21) whereas the value is 10–15 pS for lecithin membranes (8).

The values for the two-site model lead to an apparent contradiction. In this model it is required that the difference in binding energy be due to ion repulsion on double occupancy. This repulsion occurs at about 21 Å, yet at 23 Å the repulsion does not appear to be present because $k^t_{on} = 3 \times 10^7$ and $k^w_{on} = 1.2 \times 10^8$. This dilemma is retained with the "best fit" values. The rate constants say that the on-rate for the second ion is faster than for the first, yet the inverse is expected—i.e., k^w_{on} should be approximately $(K^w_b/K^t_b)\, k^t_{on}$. Two mechanisms whereby this might occur are: (*i*) if the conformational entropy of the channel is large when empty and becomes limited when occupied to give rise to a conformation with a more favorable barrier to entry and (*ii*) if the ion in the channel altered the phospholipid structure in such a way as to make access to the channel mouth more probable. The above dilemma is not present in the three-site model.

This work was supported in part by National Institutes of Health Grants GM-07195 and GM-26898 (D.W.U.) and by an Alexander von Humboldt Foundation Senior U.S. Scientist Award (D.W.U.).

1. Sarges, R. & Witkop, B. (1964) *J. Am. Chem. Soc.* **86,** 1862–1863.
2. Mueller, P. & Rudin, D. O. (1967) *Biochem. Biophys. Res. Commun.* **26,** 398–404.
3. Hladky, S. B. & Haydon, D. A. (1970) *Nature (London)* **225,** 451–453.
4. Hladky, S. B. & Haydon, D. A. (1972) *Biochim. Biophys. Acta* **274,** 294–312.
5. Myers, V. B. & Haydon, D. A. (1972) *Biochim. Biophys. Acta* **274,** 313–322.
6. Krasne, S., Eisenman, G. & Szabo, B. (1971) *Science* **174,** 412–415.
7. Bamberg, E. & Läuger, P. (1974) *Biochim. Biophys. Acta* **367,** 127–133.
8. Bamberg, E., Kolb, H.-A. & Läuger, P. (1976) in *The Structural Basis of Membrane Function* (Academic, New York), pp. 143–157.
9. Urry, D. W. (1971) *Proc. Natl. Acad. Sci. USA* **68,** 672–676.
10. Urry, D. W., Goodall, M. C., Glickson, J. D. & Mayers, D. F. (1971) *Proc. Natl. Acad. Sci. USA* **68,** 1907–1911.
11. Bamberg, E., Apell, H. J. & Alpes, H. (1977) *Proc. Natl. Acad. Sci. USA* **74,** 2402–2406.
12. Weinstein, S., Wallace, B., Blout, E. R., Morrow, J. S. & Veatch, W. (1979) *Proc. Natl. Acad. Sci. USA* **76,** 4230–4234.
13. Urry, D. W., Long, M. M., Jacobs, M. & Harris, R. D. (1975) *Ann. N.Y. Acad. Sci.* **264,** 203–220.
14. Urry, D. W. (1973) in *Conformation of Biological Molecules and Polymers—The Jerusalem Symposia on Quantum Chemistry and Biochemistry* (Israel Academy of Sciences, Jerusalem), Vol. 5, pp. 723–736.
15. Finkelstein, A. & Rosenberg, P. A. (1979) in *Membrane Transport Processes,* eds. Stevens, C. F. & Tsien, R. W. (Raven, New York), Vol. 3, pp. 73–88.
16. Koeppe, R. E., II, Berg, J. M., Hodgson, K. O. & Stryer, L. (1979) *Nature (London)* **279,** 723–725.
17. Urry, D. W., Spisni, A., Khaled, M. A., Long, M. M. & Masotti, L. (1979) *Int. J. Quantum Chem. Symp.* **6,** in press.
18. Urry, D. W., Spisni, A. & Khaled, M. A. (1979) *Biochem. Biophys. Res. Commun.* **88,** 940–949.
19. Bamberg, E. & Läuger, P. (1974) *Biochim. Biophys. Acta* **367,** 127–133.
20. Läuger, P. (1973) *Biochim. Biophys. Acta* **311,** 423–441.
21. Hladky, S. B., Urban, B. W. & Haydon, D. A. (1979) in *Membrane Transport Processes,* eds. Stevens, C. F. & Tsien, R. W. (Raven, New York), pp. 89–103.
22. Sandblom, J., Eisenman, G. & Neher, E. (1977) *J. Membr. Biol.* **31,** 383–417.
23. James, T. L. & Noggle, J. H. (1969) *Proc. Natl. Acad. Sci. USA* **62,** 644–649.
24. Swift, T. & Connick, R. (1962) *J. Chem. Phys.* **37,** 305–320.
25. Feeney, J., Batchelor, J. G., Albrand, J. P. & Roberts, G. C. K. (1979) *J. Magn. Reson.* **33,** 519–529.
26. Cornélis, A. & Laszlo, P. (1979) *Biochemistry* **18,** 2004–2007.
27. Hubbard, P. S. (1970) *J. Chem. Phys.* **53,** 985–987.
28. Bull, T. E. (1972) *J. Magn. Reson.* **8,** 344–353.
29. Lindman, B. & Forsén, S. (1976) in *NMR-Basic Principles and Progress,* eds. Diehl, P., Fluck, E. & Kosfeld, R. (Springer, Heidelberg, Germany), Vol. 12, pp. 1–368.
30. Zwolinski, B. I., Eyring, H. & Reese, C. E. (1949) *J. Phys. Chem.* **53,** 1426–1453.
31. Johnson, F. H., Eyring, H. & Polissar, M. I. (1954) in *The Kinetic Basis of Molecular Biology* (Wiley, New York), Chap. 14.
32. Parlin, B. & Eyring, H. (1954) in *Ion Transport Across Membranes,* ed. Clarke, H. T. (Academic, New York), pp. 103–118.
33. Eyring, H. & Urry, D. W. (1963) *Ber. Bunsenges. Phys. Chem.* **67,** 731–740.